

## Rearrangement of Dewar Benzene Derivatives Studied by DFT

Martin Dračínský,<sup>\*,†</sup> Obis Castaño,<sup>‡</sup> Martin Katora,<sup>†,§</sup> and Petr Bouř<sup>\*,†</sup>

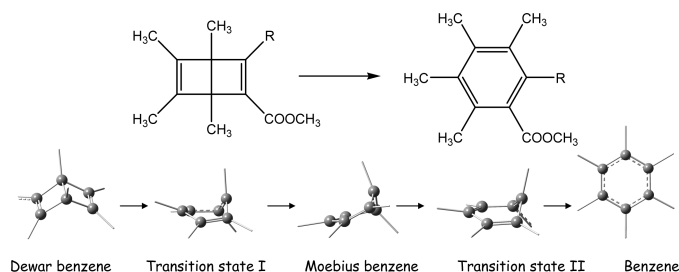
<sup>†</sup>*Institute of Organic Chemistry and Biochemistry, Academy of Sciences, 166 10 Prague, Czech Republic,*

<sup>‡</sup>*Department of Physical Chemistry, University of Alcalá, 28871 Alcalá de Henares, Madrid, Spain, and*

<sup>§</sup>*Department of Organic Chemistry, Charles University in Prague, Hlavova 8, 128 43 Praha 2, Czech Republic*

dracinsky@uochb.cas.cz, bour@uochb.cas.cz

Received September 24, 2009



Skeletal rearrangement of a series of substituted Dewar benzenes to biaryl products was studied with DFT methods. Excellent agreement of calculated free energies of activation with experimental kinetic data was achieved. Two different transition states were proposed to be involved in the rearrangement. The reaction path was studied both by static intrinsic reaction coordinate (IRC) calculations and first-principles Car–Parrinello and Born–Oppenheimer molecular dynamics. All approaches confirmed the suggested reaction mechanism.

### Introduction

The Dewar benzene (DB) **1**, a metastable benzene valence isomer, has attracted considerable interest of both synthetic and theoretical chemists. The first syntheses of Dewar benzenes were enabled in the 1960s by a clever choice of conventional reactions and/or UV irradiation of suitable precursors. By this combination, the first valence-bond isomers of benzene were soon isolated.<sup>1–4</sup> Isomerization of DBs into thermodynamically more stable normal benzenes can be achieved cleanly and quantitatively under elevated temperature or by a visible light irradiation.

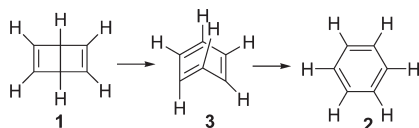
Although Dewar benzenes are in most cases unstable compounds, some of them exhibit reasonable stability even under ambient conditions. Usually, high thermal stability is

found in persubstituted DBs bearing an electron-withdrawing group.<sup>5–7</sup> A remarkable resistance to the rearrangement has also been found in a DB–ferrocene conjugate.<sup>8</sup> Recently, more stable DB derivatives have even found interesting practical applications. Typical examples include their use in the synthesis of oligophenylene macrocycles,<sup>9–11</sup> implementation as a supramolecular protecting group,<sup>12</sup> synthesis of ladderanes, and high content DB polymers.<sup>13</sup>

Particular attention has been paid to the mechanism of the ring opening accompanying the transmutation of the Dewar benzene **1** to benzene **2**. For a long time, the expected mechanism was an orbital symmetry-forbidden disrotatory path. The allowed conrotatory path was supposed to lead to an extremely strained *cis,cis,trans*-cyclohexa-1,3,5-triene **3** (*trans*-benzene, Moebius benzene) (Scheme 1).<sup>2</sup>

(1) Tamelen, E. E.; Pappas, S. P. *J. Am. Chem. Soc.* **1962**, *84*, 3789–3791.  
 (2) Tamelen, E. E. *Acc. Chem. Res.* **1972**, *5*, 186–192.  
 (3) Tamelen, E. E.; Pappas, S. P.; Kirk, K. L. *J. Am. Chem. Soc.* **1971**, *93*, 6092–6101.  
 (4) Schaefer, W.; Hellmann, H. *Angew. Chem., Int. Ed. Engl.* **1967**, *6*, 518–525.  
 (5) Schaefer, W. *Angew. Chem.* **1966**, *78*, 716–716.  
 (6) Schaefer, W.; Criegee, R.; Askani, R.; Gruener, H. *Angew. Chem.* **1967**, *79*, 54–55.  
 (7) Janková, Š.; Dračínský, M.; Císařová, I.; Katora, M. *Eur. J. Org. Chem.* **2008**, 47–51.

(8) Janková, Š.; Císařová, I.; Uhlík, F.; Štěpnička, P.; Katora, M. *Dalton Trans.* **2009**, 3137–3139.  
 (9) Ohkita, M.; Ando, K.; Yamamoto, K.; Suzuki, T.; Tsuji, T. *Chem. Commun.* **2000**, 83–84.  
 (10) Ohkita, M.; Ando, K.; Suzuki, T.; Tsuji, T. *J. Org. Chem.* **2000**, *65*, 4385–4390.  
 (11) Ohkita, M.; Ando, K.; Tsuji, T. *Chem. Commun.* **2001**, 2570–2571.  
 (12) Marsella, M. J.; Meyer, M. M.; Tham, F. S. *Org. Lett.* **2001**, *3*, 3847–3849.  
 (13) Marsella, M. J.; Estassi, S.; Wang, L. S.; Yoon, K. *Synlett* **2004**, 192–194.

**SCHEME 1. Rearrangement of Dewar Benzene 1 to Benzene 2 via *cis,cis,trans*-Cyclohexa-1,3,5-triene 3**


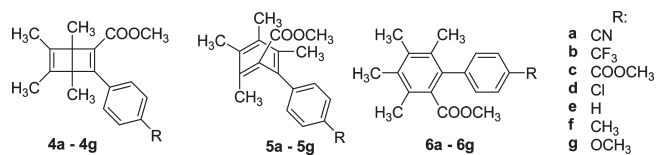
Recently, however, this simple view has been modified. When the two modes of the ring opening were studied, the commonly accepted transition state of  $C_{2v}$  symmetry on the disrotatory pathway was found to be a second-order saddle point only.<sup>14</sup> Instead, the true transition state of a  $C_s$  symmetry positioned at 3.7 kcal/mol below the  $C_{2v}$  saddle point was identified as that corresponding to the thermally allowed conrotatory electrocyclic ring opening. The disrotatory and conrotatory pathways were also studied at a higher CASSCF(10,10) level.<sup>15</sup> True transition states (i.e., those with one imaginary frequency) were found for both modes, the conrotatory transition state being 6.6 kcal/mol below the disrotatory one. Furthermore, an IRC calculation showed that the conrotatory transition state connects the Dewar benzene with benzene directly, without passing through the *cis,cis,trans*-cyclohexa-1,3,5-triene 3.

The reactivity of the Dewar benzene skeleton can further be modified by the substituents. The potential energy surface of hexamethyl Dewar benzene, for example, slightly differs from that of unsubstituted Dewar benzene.<sup>16</sup> The ring opening in the former leads to a strained *trans* conformation of hexamethylbenzene.

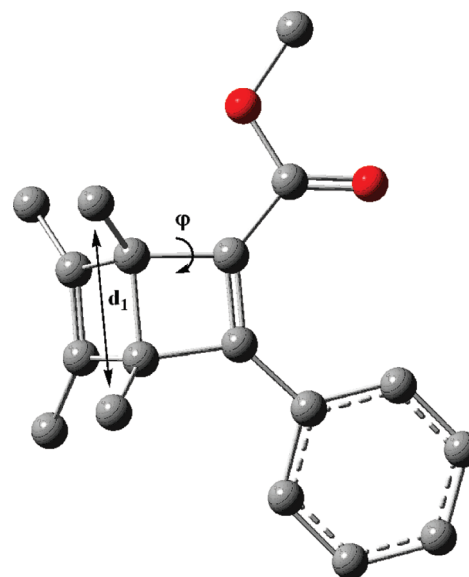
As another example, we described the synthesis of seven Dewar benzene derivatives with *para*-substituted phenylene ring (**4a–4g**, Figure 1).<sup>7</sup> We suggested a conrotatory transition state by comparison of experimental reaction rates of the Dewar benzenes thermal rearrangement (at 135.1 °C in DMSO using the NMR spectroscopy) with free activation energies  $\Delta G^\ddagger$  calculated with a polarizable continuum model of solvation.<sup>7</sup>

In the current study, we hope to shed more light on the mechanism of the rearrangement of the DBs **4a–4g** (Figures 1 and 2) and decide whether the highly strained Moebius benzene derivatives can also be involved in the rearrangement. For this purpose, we combine free energy calculations and DFT-based Car–Parrinello molecular dynamics (CPMD)<sup>17</sup> to elucidate the rearrangement dynamics.

The first-principles molecular dynamics simulations emerged as powerful techniques for simulations of chemical reactions.<sup>18–21</sup> The forces acting on the nuclei are determined by computationally expensive quantum chemical calculations, which limits the simulations to subnanosecond regime. Unfortunately, reactions even with barriers as low as



**FIGURE 1.** Investigated Dewar benzenes **4**, intermediates **5**, and benzenes **6**.



**FIGURE 2.** Dewar benzene **4e** (hydrogens are omitted for clarity). Definition of the distance  $d_1$  and torsion angle  $\phi$  ( $\text{CH}_3\text{--C--C--COO}$ ) used as reaction coordinates.

10 kcal mol<sup>-1</sup> are typically not simulated as they extend to microseconds.<sup>18</sup> To speed up the calculations, an initiate point is created by estimating reasonable atomic coordinates within the transition region.<sup>18,22–24</sup> The transition state geometry is the most obvious initial point for the reaction trajectory. As shown below, such an approach could be successfully used also for the elucidation of the DB's derivative rearrangement.

## Results and Discussion

**Intrinsic Reaction Coordinate Path.** Previously, we described<sup>7</sup> structures of seven transition states TS1, which were supposed to connect Dewar benzene derivatives **4a–4g** with the Moebius benzenes. The TS1 structures were constructed starting from the TCSCF/6-31G\* transition state<sup>14</sup> for a DB → benzene rearrangement followed by an optimization to the first-order saddle point. The transition states TS1 supposedly possess the highest energy on the rearrangement pathway.<sup>14</sup>

The IRC calculations were performed in both directions from the transition state TS1 of **4e**. In one direction, the IRC goes to Dewar benzene **4e**, while the other direction provides the Moebius benzene derivative **5e**. The Moebius derivative is associated with a very shallow minimum, separated from the transition state TS1 by 0.9 kcal/mol only

(14) Johnson, R. P.; Daoust, K. J. *J. Am. Chem. Soc.* **1996**, *118*, 7381–7385.

(15) Havenith, R. W. A.; Jenneskens, L. W.; Lenthe, J. H. *J. Mol. Struct. (THEOCHEM)* **1999**, *492*, 217–224.

(16) Norton, J. E.; Olson, L. P.; Houk, K. N. *J. Am. Chem. Soc.* **2006**, *128*, 7835–7845.

(17) Car, R.; Parrinello, M. *Phys. Rev. Lett.* **1985**, *55*, 2471–2474.

(18) Rowley, C. N.; Woo, T. K. *J. Chem. Phys.* **2007**, *126*, 024110.

(19) Dellago, C.; Bolhuis, P. G.; Chandler, D. *J. Chem. Phys.* **1998**, *108*, 9236–9245.

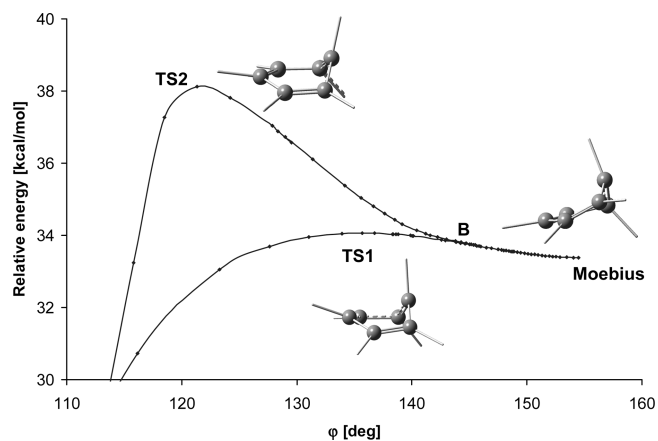
(20) Dellago, C.; Bolhuis, P. G.; Csajka, F. S.; Chandler, D. *J. Chem. Phys.* **1998**, *108*, 1964–1977.

(21) Geissler, P. L.; Dellago, C.; Chandler, D.; Hutter, J.; Parrinello, M. *Chem. Phys. Lett.* **2000**, *321*, 225–230.

(22) Bolhuis, P. G.; Chandler, D. *J. Chem. Phys.* **2000**, *113*, 8154–8160.

(23) Ma, A.; Dinner, A. R. *J. Phys. Chem. B* **2005**, *109*, 6769–6779.

(24) Pan, A. C.; Chandler, D. *J. Phys. Chem. B* **2004**, *108*, 19681–19686.



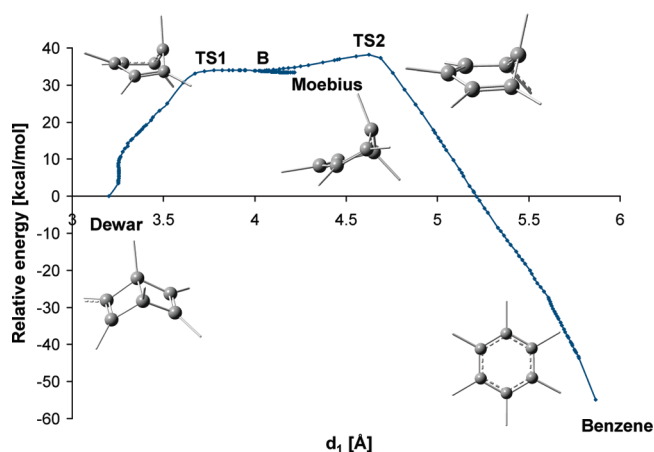
**FIGURE 3.** Calculated dependence of relative vacuum electronic energy (B3LYP/6-31G\*\*, referenced to Dewar benzene derivative) on torsional angle  $\phi$  (for definition, see Figure 2). Only the region around the transition states is depicted.

(at B3LYP/6-311+G\*\* level). A thermodynamical analysis including the solvent effects (PCM) provides a similar free energy difference between TS1 and **5e** of 1.1 kcal/mol.

The transition structure TS2, which connects the Moebius benzene **5e** and biaryl product **6e** (isomerization by  $\pi$ -bond rotation), was determined using synchronous transit-guided quasi-Newton (STQN) method as implemented in Gaussian 03.<sup>25,26</sup> Resultant transition state was by 3.5 kcal/mol higher in energy (at B3LYP/6-311+G\*\* level) than TS1. The TS2 structure thus possesses the highest energy during the Dewar benzene rearrangement. The free energy difference between TS2 and TS1 calculated with the solvent model is rather low, 0.6 kcal/mol only.

Starting from the transition state TS2, the IRC path thus in one direction provides the biaryl **6e** (final product of the rearrangement), while in the opposite direction, the IRC curve comes very close to the TS1  $\rightarrow$  Moebius IRC path (point B in Figure 3, where the dependence of the energy on the dihedral angle  $\phi$  ( $\text{CH}_3\text{-C-C-CO}$ ) is given). The dihedral angle  $\phi$  starts at  $59^\circ$  (Dewar benzene **4e**), increases to  $154^\circ$  (Moebius benzene **5e**), and falls to  $0^\circ$  (biaryl **6e**). The course of the reaction can also be observed in Figure 4, where the energy dependence on the distance  $d_1$  ( $\text{CH}_3\text{-CH}_3$ ) is depicted. The distance  $d_1$  exhibits the biggest change from all internuclear distances during the course of the rearrangement. The conrotatory transition state TS1 was found previously<sup>7</sup> for all of the Dewar benzene derivatives. According to our knowledge, however, the transition state TS2 observed in this work has not been described yet.

The relative free energies of the ground and transition states TS1 and TS2 are summarized in Table 1. The calculated free energies of activation (differences between free energies of TS2 and the Dewar benzene derivative) are in a very good agreement with those obtained experimentally. The two transition states TS1 and TS2 are energetically very close. This explains the previously observed good correlation between the TS1 and experimental  $\Delta G^\ddagger$  values.<sup>7</sup> We can also see that TS2 always has higher energy than TS1, and thus



**FIGURE 4.** Calculated dependence of relative vacuum electronic energy (B3LYP/6-31G\*\*, referenced to Dewar benzene derivative) on the internuclear distance  $d_1$  within the whole range.

TS2 limits the reaction rate. The differences between calculated and experimental free energies of activation are 0–0.6 kcal/mol. The free energies of activation in vacuum (Table 1) are always about 2 kcal/mol higher than those in DMSO. This can be explained by the fact that TS2 has a larger dipole moment (see Supporting Information) than the Dewar benzenes; therefore, TS2 is stabilized by polar solvents. As can also be seen from Table 1, electron-donating substituents (e.g., the methoxy group) stabilize the Dewar benzene and slow down its rearrangement to the biaryl derivative. As shown previously, the rearrangement rates correlate very well with the *para*- $\sigma$  Hammett constants.<sup>7</sup>

**CPMD Trajectories.** We also performed Car–Parrinello molecular dynamics runs to generate reaction trajectories from the transition states structures TS1 and TS2 and from the Moebius benzene derivative of **4e** using random starting velocities based on Boltzmann distribution at 300 K. The simulation temperature was lower than the experimental one (408 K) because, when higher temperature was used during the CPMD runs, starting structures relaxed to the products during the equilibration period in some simulations. Lowering the temperature thus enabled us to better capture reaction intermediates for the same reaction mechanism. The trajectories were run forward and backward in time by 5000 to 20 000 time steps (4 au per time step).

The Car–Parrinello molecular dynamics was performed with the BLYP GGA functional for computational convenience. For example, the same computation would be about 50 times more time-expensive if performed with the hybrid B3LYP method. It is generally accepted that the performance of BLYP and B3LYP is comparable. Nevertheless, to be sure that a functional variation does not significantly change the potential energy surface, we calculated the energies of Dewar benzene **4e**, Moebius benzene **5e**, both transition states, and the biaryl derivative **6e** in Gaussian with the B3LYP and BLYP functionals and in the CPMD program with the BLYP functional. We also optimized the geometry of all five structures with the BLYP functional implemented in Gaussian. As can be seen in Table 2, all methods gave similar relative energies; in all cases, the transition state TS2 had the largest energy. Structures of TS1, TS2, and Moebius benzene optimized with both functionals were used as starting points for

(25) Peng, C.; Ayala, P. Y.; Schlegel, H. B.; Frisch, M. J. *J. Comput. Chem.* **1996**, *17*, 49–56.

(26) Peng, C.; Schlegel, H. B. *Isr. J. Chem.* **1994**, *33*, 449–454.

**TABLE 1.** Calculated (B3LYP/6-311+G\*\*, Implicit DMSO) Relative Free Energies of Dewar Benzene Derivatives, TS1, TS2, Moebius Benzenes, and Biaryl Products of the Rearrangement, and Calculated and Experimental Free Energies of Activation of the Dewar Benzene Rearrangement

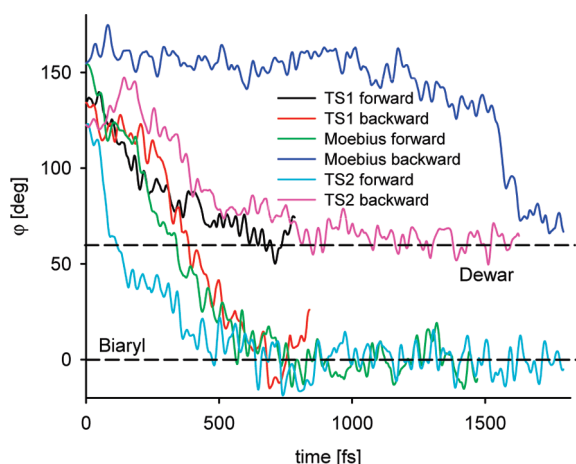
	R	Dewar <sup>a</sup>	TS1 <sup>a</sup>	Moebius <sup>a</sup>	TS2 <sup>a</sup>	biaryl <sup>a</sup>	$\Delta G^\ddagger_{\text{vacuum}}{}^a$	$\Delta G^\ddagger_{\text{DMSO}}{}^a$	$\Delta G^\ddagger_{\text{exp}}{}^{a,b}$
4a	CN	0	29.8	27.7	30.2	-58.5	32.9	30.2	<b>30.8</b>
4b	CF <sub>3</sub>	0	30.4	27.9	30.8	-58.1	33.3	30.8	<b>31.2</b>
4c	COOMe	0	30.3	27.8	30.6	-58.1	33.0	30.6	<b>31.2</b>
4d	Cl	0	30.7	28.6	31.2	-58.0	33.6	31.2	<b>31.6</b>
4e	H	0	31.0	28.9	31.6	-58.0	33.8	31.6	<b>31.9</b>
4f	Me	0	31.6	29.2	32.0	-57.6	33.9	32.0	<b>32.0</b>
4g	OMe	0	31.9	29.4	32.2	-56.8	34.2	32.2	<b>32.3</b>

<sup>a</sup>Energies in kcal/mol. <sup>b</sup>From ref 7.

**TABLE 2.** Relative Vacuum Electronic Energies of Dewar Benzene 4e, TS1, TS2, Moebius Benzene 5e, and the Biaryl Product 6e of the Rearrangement Calculated with Different Methods<sup>a</sup>

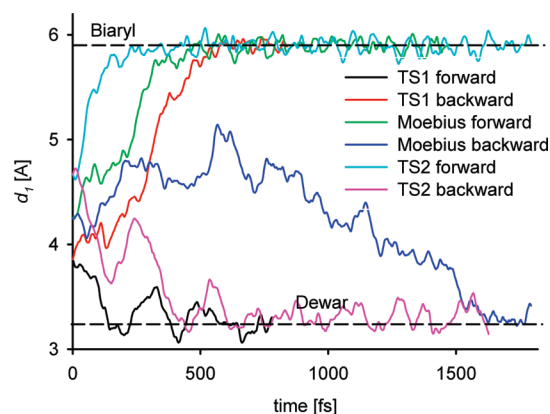
	B3LYP <sup>b,c</sup>	BLYP <sup>b,c</sup>	BLYP <sup>b,d</sup>	BLYP <sup>c,e</sup>	BLYP <sup>d,e</sup>
4e	0.00	0.00	0.00	0.00	0.00
TS1	32	28	27	28	27
5e	32	27	27	27	27
TS2	36	31	30	31	30
6e	-55	-54	-55	-54	-55

<sup>a</sup>Energies in kcal/mol. <sup>b</sup>Geometry optimized B3LYP/6-311+G(d,p). <sup>c</sup>Gaussian (G03) basis set. <sup>d</sup>Planar wave (CPMD) basis set. <sup>e</sup>Geometry optimized BLYP/6-311+G(d,p).

**FIGURE 5.** Example of the angle  $\varphi$  dependence (for definition, see Figure 2) on the time of the CPMD propagation. Simulations started from transition state TS1 (black and red curves), from Moebius benzene (green and blue curves), and from transition state TS2 (cyan and pink curves). Equilibrium torsions  $\varphi$  (from static Gaussian calculations) for Dewar benzene 4e and for biaryl derivative 6e are shown as the dashed lines.

generating CPMD trajectories. One set of trajectories was initialized with random velocities of all atoms, and no extra energy was given in the reaction coordinate. The second set of trajectories started from the same geometries but opposite momenta than those used in the first set. In total, 12 CPMD runs were done.

The CPMD starting from TS1 led to Dewar benzene derivative in one time direction and to biaryl product in the reverse direction. An example of the course of the dynamics can be observed in the time dependence of values of the selected internal coordinates (Figure 5 for  $\varphi$  and Figure 6 for  $d_1$ ). Apparently, the reaction did not pass through the Moebius benzene because the torsion angle  $\varphi$  did not increase during the simulation. This suggests that the

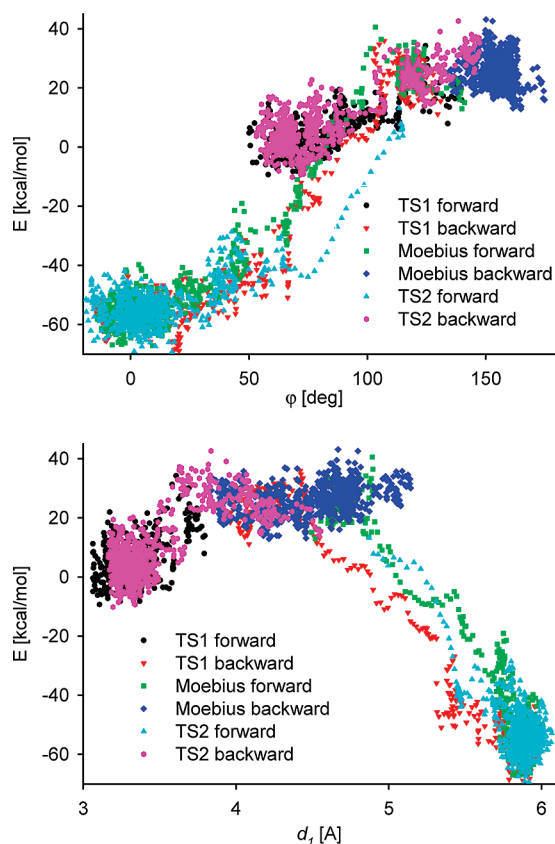
**FIGURE 6.** Examples of the distance  $d_1$  dependence (for definition, see Figure 2) on the time of the CPMD simulations. Simulations started from transition state TS1 (black and red curves), from Moebius benzene (green and blue curves), and from transition state TS2 (cyan and pink curves). Equilibrium torsions  $\varphi$  (from static Gaussian calculations) for Dewar benzene 4e and for biaryl derivative 6e are shown as the dashed lines.

Moebius benzene derivative is not necessarily the rearrangement reaction intermediate.

In the simulations starting from Moebius benzene derivative, the Moebius benzene remained stable in the simulations for 0.2–2 ps and then it rearranged to the Dewar benzene or biaryl product. From that follows that the Moebius benzene derivative can exist for a limited time as a distinct species.

The simulation starting from TS2 optimized at B3LYP/6-311+G(d,p) level led always to the biaryl product (data not shown) even when the initial velocities of the atoms were set to follow the vibrational normal mode coordinate (with negative frequency) corresponding to the reaction path. The harmonic normal modes were calculated in Gaussian, and the velocities were rescaled to the temperature of 300 K. This can probably be explained by a slightly different potential energy surface in the vicinity of TS2 obtained with B3LYP functional by Gaussian and the surface followed in the CPMD/BLYP simulations. A minor change around the transition state can move the molecule from the saddle above a deep valley, and the CPMD simulation therefore leads to the biaryl product. When the simulations were started from the TS2 geometry optimized at BLYP/6-311+G(d,p) level, it led to the biaryl product in one temporal direction and to the Dewar benzene in the other direction. In the simulation leading to the Dewar benzene, the molecule passed through the Moebius benzene region (torsion angle  $\varphi$  close to 150°).

Dependence of the relative Kohn–Sham energy, which is the equivalent of potential energy in classical MD

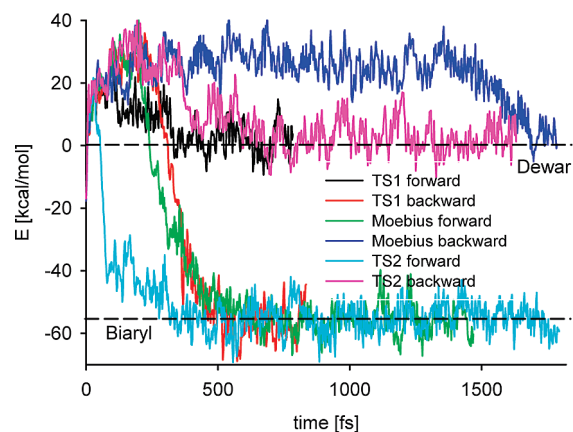


**FIGURE 7.** Dependence of relative Kohn–Sham energy (referenced to Dewar benzene derivative) of CPMD trajectory snapshots on the torsion angle  $\varphi$  (top) and on the distance  $d_1$  (bottom).

(referenced to Dewar benzene derivative), of the CPMD trajectory snapshots on the torsion angle  $\varphi$  and the distance  $d_1$  is depicted in Figure 7. The dependence agrees very well with the dependence obtained from the static IRC calculations (depicted in Figures 3 and 4).

The overall progress of the rearrangement reaction during the CPMD simulations can be also observed in Figure 8, where dependencies of the relative Kohn–Sham energy (referenced to Dewar benzene derivative) on the time of CPMD simulation are shown. The average energies can be well compared with the IRC results (Figure 3); the relatively large oscillations ( $\pm 10$  kcal/mol) suggest a significant energy redistribution enabling the chemical reactions.

To exclude an influence of the MD propagation algorithm on the reaction mechanism and energetic, we also performed constrained Born–Oppenheimer molecular dynamics (BOMD) simulations. Note that, unlike in CPMD, in BOMD the electronic wave function is optimized at every time step. Additionally, constraints on reaction coordinates ( $d_1$ ,  $\varphi$ ) were linearly added to the Car–Parrinello Lagrangian according to the blue moon ensemble prescription.<sup>27</sup> Dewar benzene derivative **4e** was the starting structure in the simulations. Obtained results, however, were very similar as observed in the free CPMD simulations described above. When only the distance  $d_1$  was constrained to increase during the simulation, it led to a disrotatory mechanism of the Dewar benzene rearrangement with the Kohn–Sham energy



**FIGURE 8.** Dependence of the relative Kohn–Sham energy (referenced to Dewar benzene derivative) on the time of the CPMD simulations.

barrier of 40 kcal/mol (about 10 kcal/mol higher than conrotatory CPMD simulations). When both the distance  $d_1$  and the torsion angle  $\varphi$  were constrained, the simulation led to the conrotatory Dewar benzene rearrangement. It should be noted that for multidimensional problems reducing the reaction coordinate to a distance or an angle might not be adequate;<sup>27</sup> in our case, the agreement of the CPMD and BOMD simulations, however, such approximation seems reasonable.

## Conclusions

By theoretical simulations, we have found two different transition states on the reaction path of the Dewar benzene rearrangement. The state TS1 connects Dewar benzene with its Moebius valence isomer, while TS2 connects Moebius benzene with a biaryl product of the rearrangement. The two IRC curves meet in point B, so that the two valleys coming from TS1 and TS2 unite and lead to Moebius benzene. The TS2 represents the highest barrier during the rearrangement. The computations confirmed the experimental observations that the more electron-donating substituents are attached to the Dewar benzene the slower is the rearrangement (the calculated barrier is higher). This is also in agreement with previous observation where electron-donating substituents slowed down the conrotatory rearrangement of cyclobutadiene.<sup>28</sup>

First-principle Car–Parrinello molecular dynamics simulations excellently confirmed the static IRC calculations. Both methods indicated that both transition states as well as Moebius derivative can connect the Dewar benzene derivative with the biaryl product.

Although more simulations would be necessary to obtain relative free energies of the rearrangement, we could get a good qualitative insight by analyzing a limited number of trajectories. The CPMD relative Kohn–Sham energies are in very good agreement with the free energies obtained by the static Gaussian calculations (see Figures 7 and 8). The solvent environment caused modest changes of the relative energies but does not seem to significantly change the

(27) Sprik, M.; Ciccotti, G. *J. Chem. Phys.* **1998**, *109*, 7737–7744.

(28) Niwayama, S.; Kallel, E. A.; Spellmeyer, D. C.; Sudu, C.; Houk, K. N. *J. Org. Chem.* **1996**, *61*, 2813–2825.

reaction mechanism. We can thus conclude that the ab initio calculations brought an important insight in the Dewar benzene chemistry and allowed us to better interpret the experimental data.

### Computations

The stationary point searches and IRC calculations were carried out using the Gaussian 03 software package.<sup>29</sup> Full geometry optimizations verified by analytical vibrational frequency analyses were carried out for all minima and transition structures with the Becke3LYP<sup>30,31</sup> functional and a standard 6-311+G(d,p) basis set. The ground state structures were found to be true minima with no imaginary frequencies, while the transition structures were first-order saddle points (i.e., with a single imaginary frequency). The geometry optimizations and the frequency calculations were done in vacuum. As the dipole moments of the molecules are significant and polar solvent (such as dimethylsulfoxide) can influence the rate of the rearrangement, the calculations for the optimized structures were completed by single point estimations of energy comprising a continuum solvent model. The polarizable continuum model<sup>32</sup> (PCM) and DMSO solvent were chosen, as implemented in Gaussian. The free energy in solution was calculated as  $\Delta G_{\text{DMSO}} = \Delta G_{\text{vacuum}} - \Delta E_{\text{vacuum}} + \Delta E_{\text{DMSO}}$ , where  $\Delta G_{\text{vacuum}}$  and  $\Delta E_{\text{vacuum}}$  are the free energy and electronic energy differences in vacuum, and  $\Delta E_{\text{DMSO}}$  is the electronic energy difference in solution. The IRC calculations were performed at

(29) Frisch, M. J.; Trucks, G. W.; Schlegel, H. B.; Scuseria, G. E.; Robb, M. A.; Cheeseman, J. R.; Montgomery, J. A., Jr.; Vreven, T.; Kudin, K. N.; Burant, J. C.; Millam, J. M.; Iyengar, S. S.; Tomasi, J.; Barone, V.; Mennucci, B.; Cossi, M.; Scalmani, G.; Rega, N.; Petersson, G. A.; Nakatsuji, H.; Hada, M.; Ehara, M.; Toyota, K.; Fukuda, R.; Hasegawa, J.; Ishida, M.; Nakajima, T.; Honda, Y.; Kitao, O.; Nakai, H.; Klene, M.; Li, X.; Knox, J. E.; Hratchian, H. P.; Cross, J. B.; Bakken, V.; Adamo, C.; Jaramillo, J.; Gomperts, R.; Stratmann, R. E.; Yazyev, O.; Austin, A. J.; Cammi, R.; Pomelli, C.; Ochterski, J. W.; Ayala, P. Y.; Morokuma, K.; Voth, G. A.; Salvador, P.; Dannenberg, J. J.; Zakrzewski, V. G.; Dapprich, S.; Daniels, A. D.; Strain, M. C.; Farkas, O.; Malick, D. K.; Rabuck, A. D.; Raghavachari, K.; Foresman, J. B.; Ortiz, J. V.; Cui, Q.; Baboul, A. G.; Clifford, S.; Cioslowski, J.; Stefanov, B. B.; Liu, G.; Liashenko, A.; Piskorz, P.; Komaromi, I.; Martin, R. L.; Fox, D. J.; Keith, T.; Al-Laham, M. A.; Peng, C. Y.; Nanayakkara, A.; Challacombe, M.; Gill, P. M. W.; Johnson, B.; Chen, W.; Wong, M. W.; Gonzalez, C.; Pople, J. A. *Gaussian 03*, revision C.02; Gaussian, Inc.: Wallingford, CT, 2004.

(30) Lee, C.; Yang, W.; Parr, R. G. *Phys. Rev. B* **1988**, *37*, 785–789.

(31) Becke, A. D. *J. Chem. Phys.* **1993**, *98*, 5648–5652.

(32) Mennucci, B.; Cancès, E.; Tomasi, J. *J. Phys. Chem. B* **1997**, *101*, 10506–10517.

B3LYP/6-31G(d,p) level. Analytical force constants were also calculated at every point of the IRC path.

The transition structures obtained were subjected to Car–Parrinello molecular dynamic runs performed with the aid of the CPMD<sup>33</sup> software package. The molecules (transition states TS1 and TS2 found on the IRC path and Moebius benzene, geometries of which were determined by the Gaussian calculations) were placed in a periodic box  $20 \times 20 \times 20$  Å in size. This ensures that the periodic images needed for CPMD are well-separated from each other and do not interact. The Martyna and Tuckerman Poisson solver<sup>34</sup> was used for the isolated systems.<sup>35</sup> A time step of 0.09676 fs (4 atomic units), energy cutoff of 25 Ry, the BLYP<sup>31</sup> functional, Vanderbilt ultrasoft pseudopotentials,<sup>36</sup> and electron mass of 600 au were used in all of the CPMD calculations. The initial configuration was relaxed by five short dynamic runs comprising 200 steps. After each run, the system was quenched to the Born–Oppenheimer surface by reoptimizing the wave function. Then longer 0.8–2 ps production runs were performed. The temperature of 300 K was maintained with the Nosé–Hoover algorithm,<sup>37–40</sup> which also kept the system in the canonical (NVT) ensemble. From the long runs, trajectory snapshots were saved every 20 time steps.

**Acknowledgment.** Financial support from GAAV through projects KJB400550903, IAA400550702, and IAA401110805, DGES through project CTQ2006-07643, and MŠMT project MSM0021620857 is acknowledged, and the authors thank Dr. Raúl Palmeiro for fruitful discussions and recommendations.

**Supporting Information Available:** Cartesian coordinates and energies, enthalpies, entropies, and dipole moments for all calculated compounds at the B3LYP/6-311+G\*\* level, Cartesian coordinates and energies of compounds **4e**, **5e**, **6e**, TS1, and TS2 calculated at BLYP/6-311+G\*\* level. This material is available free of charge via the Internet at <http://pubs.acs.org>.

(33) CPMD, version 3.11; IBM Corp.: Stuttgart, Germany, 2006; <http://www.cpmid.org>.

(34) Martyna, G. J.; Tuckerman, M. E. *J. Chem. Phys.* **1999**, *110*, 2810–2821.

(35) Hockney, R. W. *Methods Comput. Phys.* **1970**, *9*, 136–211.

(36) Vanderbilt, D. *Phys. Rev. B* **1990**, *41*, 7892–7895.

(37) Hoover, W. G. *Phys. Rev. A* **1985**, *31*, 1695–1697.

(38) Nose, S.; Klein, M. L. *Mol. Phys.* **1983**, *50*, 1055–1076.

(39) Nose, S. *Mol. Phys.* **1984**, *52*, 255–268.

(40) Nose, S. *J. Chem. Phys.* **1984**, *81*, 511–519.